

Atom-driven multistability in an optomechanical cavity under broken \mathcal{PT} -symmetry

Hou Ian¹

¹*Institute of Applied Physics and Materials Engineering, FST, University of Macau, Macau*

An optical field inside a Fabry-Perot cavity would exhibit multistability either when an atomic medium, acting as a classical dielectric, is filled into the cavity or when the cavity becomes optomechanical where one reflecting end becomes movable. An external laser is essential in both cases to drive the cavity mode out of the zero equilibrium state. We study the equilibrium states of an atom-filled optomechanical cavity, where the atoms are considered a collective two-level systems as well as an active component that replaces the role of the driving laser. Multistability is found when the atomic ensemble is lossy, for which the complex atom-photon coupling breaks the \mathcal{PT} -symmetry of the system Hamiltonian and matches in a periodic pattern to the frequencies and the linewidths of the cavity mode and the collective bosonic mode of the atoms. We show an input-output hysteresis cycle between the atomic mode and the cavity mode to demonstrate the driving role the atoms replace an extra-cavity laser.

I. INTRODUCTION

When a nonlinear medium is filled inside a Fabry-Perot (FP) cavity interferometer, an incident laser through the cavity experiences optical bistability [1–3]. From a classical point of view, it is the dual effective round-trip paths inside the nonlinear medium that permits the incident laser admit two stable values of transmittivity, the determination of which depends on the intensity of the laser [4]. The multi-valued branching of the transmittivity forms a hysteresis cycle typical of the bistability behavior in the laser input-output power diagram [1]. When the nonlinear medium has Zeeman sublevels that are split by an optical pumping, the lower branch of the hysteresis cycle breaks up into two, making the system tristable [5]. In the case of ring cavity, even multistability is achievable if the filled medium consists of three-level atoms [6].

This kind of optical multistability is not unique to atom-filled FP cavities. The role played by the nonlinear atomic medium can be substituted by a movable mirror placed at one end of the cavity [7–9]. The mirror's oscillation deforms the cavity and induces a Kerr-like nonlinear dispersion, giving rise to a similar hysteresis of bistability induced by the photon-phonon interaction in radiation pressure [10]. Since then, interests in the stability problem is revived [11, 12] under the context of cavity optomechanics [13]. The mechanical multistability problem has ramified into many branches of studies, including optomechanical instability [14], optimal regime for entanglement [15, 16], cavity assisted spin-orbit coupling [17], and optomechanically induced transparency [18–20].

In this paper, we find out how multistable states arise when both an atomic medium and an oscillating mirror are present, where the optomechanical cavity is essentially a quantum tripartite AOM system composing of the collective bosonic mode of the *atoms*, the *optical* cavity mode, and the *mechanical* resonator mode of the mirror. Considering the fact that atoms in cavities can initiate strong coupling to both the cavity field [21] and the mirror [22], strong interfering motions are expected to appear between the atomic medium and the oscillating mirror. It has been shown that the mirror can be bistable [23] or multistable [12].

Considering the atoms as two-level systems, our study here,

however, is to test whether the motion of the atoms alone can drive the optomechanical cavity into multistable equilibria, where the external laser driving is eliminated, since it is proven that the atoms' excitations can vibrate like a resonator [24] and provide effective driving and squeezing to the mirror [25]. Presented in Sec. II below, this tripartite coupling model without external driving regards the motions of the atoms through a collective bosonic mode whose interaction with the cavity mode is lossy.

As we shall demonstrate in Sec. III, it is found that multistability arises only when this lossy bosonic mode, which breaks the \mathcal{PT} -symmetry of the tripartite system Hamiltonian [28], has an atom-photon coupling that matches with its own eigenfrequency and linewidth as well as the frequency and linewidth of the cavity mode. Even though they do not bump energy into the cavity but on the contrary absorb energy from the cavity, the atoms as an active component strikes a gain-loss balance to the rest two components. The gain-loss balance has recently proven to be central to the study of coupled optomechanical ring cavities [29–31], which can not only initiate phonon lasing [29] but also trigger a chaotic motion [32].

In Sec. IV, we show the hysteresis cycles, which are prevalent in multistable cavity systems, peculiar to the \mathcal{PT} -asymmetric AOM system and discuss their properties. The conclusions are given finally in Sec. V.

II. COUPLING MECHANISM

We consider the model illustrated in Fig. 1. A mirror of effective mass m , whose displacement from the equilibrium position is denoted by x and conjugate momentum denoted by p , is undergoing an oscillating motion of frequency ω_M . The motions of the mirror and the atoms are coupled via the cavity field of frequency ω_0 : on one side, the cavity field acts on the mirror through the radiation pressure η initiated by the small displacement x of the mirror that deforms the cavity volume V ; on the other, the cavity field couples with the two-level atoms through dipole-field interaction whose strength $g_j = \Omega\mu \sin k_j Q_j / \sqrt{(\omega_0 + \eta x)\epsilon_0 V(1+x)}$ with $\hbar = 1$ is parametrized by the cavity geometry, where Q_j denotes the

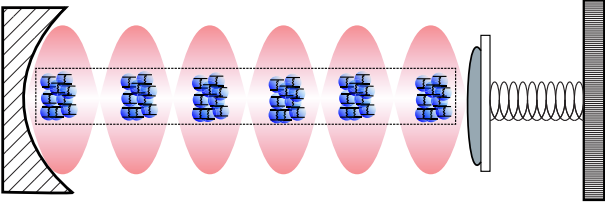


Figure 1: (Color online) Illustration of the tripartite optomechanical cavity with the active parts colored: each blue disk is a two-level atom of uniform eigenenergy Ω that couples to a red-shaded single-mode cavity field of frequency ω_C . The dark-gray tinted cap is the oscillating mirror of frequency ω_M that interacts through radiation pressure on the reflective mirror coating at the right cavity wall.

position, k_j the wave number, Ω the uniform atomic level spacing, ω_0 the cavity mode frequency, and μ the uniform dipole moment of each atom.

For the densely packed atoms we consider here, particularly when they form a Bose-Einstein condensate [26], the uniformity of the strength g_j renders the atomic ensemble a Hopfield quantum dielectric [25, 27]. At low-energy, the atoms are sparsely excited and these excitations can be collectively described by a single bosonic mode b that shares the same eigenenergy Ω with the N individual atoms. This model leads the atom-field coupling rescaled to

$$G = \sqrt{ng} = \sqrt{\frac{N}{2\omega_0\epsilon_0V}}\Omega\mu \quad (1)$$

where $n = N/V$ denotes the density of packed atoms. In other words, when the scale of the atom-field detuning and the deformation of the cavity volume caused by the displacement x is relatively small, the radiation pressure has no direct effect on the distribution of the atoms.

Nonetheless, the cavity field acts as an optical lattice that distributes the atoms periodically along the cavity axis [17, 33]. The atoms consequently forms a grating that diffracts the cavity field, leading to an optical gain [34]. To be exact, the cavity field acts simultaneously as a quasiresonant pump field to the atoms, which produces collective atomic recoil lasing without population inversion [35]. The recoil lasing is reflected by a gain term with real positive coefficient in the atom-cavity coupled equations of motion [36].

To observe more directly the relation between the dynamic gain-loss and \mathcal{PT} -symmetry, we introduce a hypothetical “phase factor” $e^{i\phi}$ in the tripartite AOM system Hamiltonian

$$H = \Omega b^\dagger b + \omega_0 a^\dagger a + \frac{p^2}{2m} + \frac{1}{2}m\omega_M^2 x^2 - \eta x a^\dagger a + Ge^{i\phi}(b^\dagger a + ba^\dagger). \quad (2)$$

The real part of $Ge^{i\phi}$ would then associate with the usual dispersion while its imaginary part associates with an atom-cavity gain in the corresponding equations of motion. Writing the two fast-varying modes under the rotating frame of the cavity, i.e. $a \rightarrow ae^{-i\omega_0 t}$ and $b \rightarrow be^{-i\omega_0 t}$, these equations of

motion read

$$\ddot{x} + \Gamma\dot{x} + \omega_M^2 x = \frac{\eta}{m}a^\dagger a, \quad (3)$$

$$\dot{a} = i\eta x a - \kappa a - iGe^{i\phi}b, \quad (4)$$

$$\dot{b} = -i\delta b - \gamma b - iGe^{i\phi}a. \quad (5)$$

where $\delta = \Omega - \omega_0$ denotes the atom-cavity detuning, Γ the decay rate of the mirror, κ the linewidth of the cavity field, and γ the relaxation rate of the bosonic mode of the atoms. Decoupling Eqs. (4)-(5), we note that the “phase” ϕ taking values away from the period $2n\pi$ would lead to a gain to the cavity mode a when breaking the \mathcal{PT} -symmetry of the Hamiltonian Eq. (2) about the steady state $\langle x \rangle = \eta | \langle a \rangle |^2 / m\omega_M^2$.

III. DYNAMIC MULTISTABILITY

A. Stability branching of mirror

To see $\langle x \rangle$ can admit non-zero values, we combine the steady-state solutions of Eqs. (3)-(5) to arrive at a gain-loss balance equation

$$\kappa\gamma + \delta\eta \langle x \rangle + G^2 e^{2i\phi} + i[\kappa\delta - \gamma\eta \langle x \rangle] = 0 \quad (6)$$

Introducing the compound gain-loss ratio

$$\rho = \frac{G^2}{\kappa^2} \cdot \frac{G^2}{\gamma^2 + \delta^2} \quad (7)$$

of the AOM system, we derive from the balance equation that only when the atom-cavity phase ϕ matches a periodic value

$$\phi_0 = \frac{1}{2} \left[\tan^{-1} \frac{\delta \pm \gamma\sqrt{\rho-1}}{\gamma \mp \delta\sqrt{\rho-1}} + k\pi \right] \quad (8)$$

where $k \in \mathbb{Z}$, then the mirror can admit two non-zero steady states

$$\langle x \rangle = \pm \frac{\kappa}{\eta} \sqrt{\rho-1}. \quad (9)$$

Since Ω and γ are always greater than zero, the fraction in the arctangent of Eq. (8) ensures that multiples of 2π would be not admissible for ϕ_0 , showing that multistability only appears when \mathcal{PT} -symmetry is broken. Further, the factor $\sqrt{\rho-1}$ in Eq. (8) and Eq. (9) implies that multistability is admissible only when the atom-cavity interaction G enters the strong-coupling regime to overcome the losses due to the cavity leakage and the atomic relaxation and to offset the frequency of the atomic mode.

Figure 2 shows a semilog plot of $\langle x \rangle$ against G over a wide range from $N = 1$ to $N = 10^7$, where the parameters are set to experimentally accessible values [24]. That is, $\kappa = 1.3$ MHz, $\gamma = 3.0$ MHz, $\eta = \sqrt{1.8}\kappa$, $g = 10.9$ MHz, and $\delta = 32$ GHz. Setting off from $\langle x \rangle = 0$, the non-zero values admissible by $\langle x \rangle$ starts branching at $\rho = 1$, which occurs at $G = 204$ MHz in the plot, into two branch cuts with different behaviors near and far from the singular point. In the

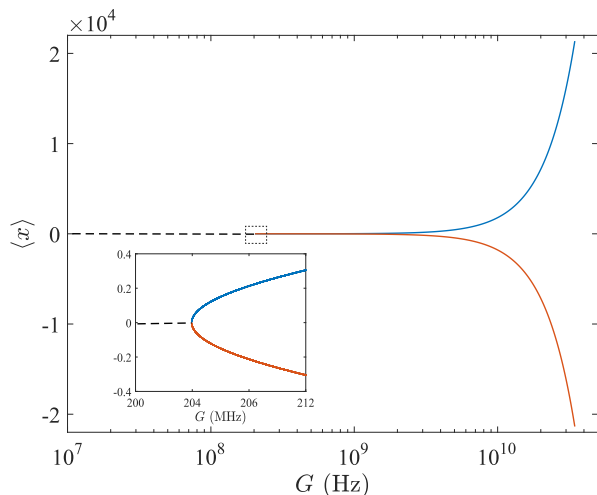


Figure 2: (Color online) Branching of the steady state $\langle x \rangle$ as a function of the coupling strength G , plotted with abscissa in log scale. The inset shows the magnified area in the dashed box with abscissa in normal scale.

far right where $G \gg 1$, $\langle x \rangle$ is quadratic whereas in the near range, $\langle x \rangle$ is parabolic. Specifically, seeing the two branches are monotonic functions of G , we can define the saddle point where $d^2 \langle x \rangle / dG^2 = 0$ at

$$G = [3\kappa^2(\gamma^2 + \delta^2)]^{1/4} \quad (10)$$

to be the separating point between the quadratic region and the parabolic region.

It should be remarked that, in classical steady-state models for FP cavities, the intra-cavity atoms act as a dielectric that feeds a nonlinear response to the cavity mode. Regarding the fields at the two reflective mirrors as input and output ends, respectively, one recognizes that the nonlinear response lets the fields traverse multiple times in the dielectric medium that associates with a field-quadrature dependent high-order susceptibility. The input-output response equation therefore translates to a high-order algebraic equation of the transmitted field, where the first-order (linear) response corresponds to the zero stable state and the higher-order responses correspond to the non-zero stable states.

In steady-state models for optomechanical cavities, one has similar high-order algebraic equations for multistability except its variable becoming the coordinate of the mirror, where the cavity field can be regarded as the input. In other words, the determination of $\langle x \rangle$ is established upon the determination of the steady states $\langle a \rangle$ of the cavity mode. This is equivalent to the tripartite model here under Bogoliubov approximation for atomic condensates, i.e. $\langle b \rangle = \langle b^\dagger \rangle \rightarrow \sqrt{N}$ while the time-dependence only exists in fluctuating terms $\delta b(t)$ and $\delta b^\dagger(t)$. Given the approximation, Eq. (5) can be ignored when considering the steady-state solutions and Eq. (4) reduces the solution of $\langle a \rangle$ to the form of a normal laser driving, $\mathcal{E}/(\kappa - i\eta \langle x \rangle)$, where $\mathcal{E} = G\sqrt{N}$ and ϕ assumes the value of $\pi/2$. Note that such a consideration only shows a formal resemblance of the low-order response of an atomic conden-

sate to an external driving. It does not retrieve the steady state induced by external driving since the limiting process does not recover the Hermitean and thus \mathcal{PT} -symmetric interaction Hamiltonian $i(a - a^\dagger)$ under the rotating frame. $\pi/2$ is not an admissible value given by Eq. (8).

Henceforth, the atomic ensemble depicted collectively by the bosonic mode does not play an active role in generating the nonlinear response to obtain non-zero stable states to $\langle x \rangle$. It instead feeds a complex response arising from its composite gain and loss back to the cavity mode. This response cancels the degree of freedom in the cavity mode exactly when the gain-loss balance is obtained, i.e. when the phase angle ϕ matches ϕ_0 given in Eq. (8), where $\langle x \rangle$ breaks off from the zero state along the two branches given in Eq. (9). The steady states of $\langle x \rangle$ is thus determined not by the cavity steady state $\langle a \rangle$, but by the system parameters $\{G, \delta, \gamma, \kappa, \eta\}$. Rather, the cavity steady state $\langle a \rangle$ is conversely determined by $\langle x \rangle$.

Put in algebraic terms, the vector $\langle \mathbf{u} \rangle = (\langle a \rangle, \langle b \rangle)$ of the steady states of the cavity mode and the atomic bosonic mode is determined by Eqs. . Written in matrix form, the system of equations is the homogeneous equation

$$\begin{bmatrix} \kappa - i\eta \langle x \rangle & iGe^{i\phi} \\ iGe^{i\phi} & i\delta + \gamma \end{bmatrix} \langle \mathbf{u} \rangle = 0, \quad (11)$$

which admits non-zero solutions only when the matrix is degenerate. The branches plotted in Fig. 2 is the degenerate curve of the matrix when the phase angle ϕ is fixed on one of values admissible by Eq. (8).

B. Phase-matching for gain-loss balance

When $\langle x \rangle$ takes values along the branches for any given atom-cavity coupling G , the phase angle ϕ has to match with ϕ_0 determined by the decay rates of the cavity and the atoms and the detuning between them. This hypothetical angle determines how the atom-cavity interaction breaks down into the real and the imaginary parts and thus decides whether the atoms are in the domain of gain or loss for the cavity field. Shown in Fig. 3 with $k = 0$, this phase-matching angle extends a wide range over the detuning δ , where the parameters are assumed the same values taken by the plot in Fig. 2. The two curves correspond to the two diverging branches of the steady state $\langle x \rangle$ and they meet at two points $\delta = \pm \sqrt{(G^4/\kappa^2) - \gamma^2}$ for which $\sqrt{\rho - 1} = 0$, which is the diverging point of $\langle x \rangle$.

To determine whether the atom-cavity coupling is undergoing a gaining process of a lossy processing for the cavity field at a given phase-matching angle ϕ_0 , we examine the sign of the real part of the term associated with the coefficient $iGe^{i\phi}$ in the equations of motion. But seeing Eq. (4) and Eq. (5) cannot be decoupled into a second-order differential equation of the cavity mode a alone, we determine the characteristics of the motion of a in the dual space of time through a Laplace transform.

Laplace transforming Eq. (5), we find

$$\mathfrak{b}(s) = \frac{-iGe^{i\phi} \mathfrak{a} + \mathfrak{F}}{s + i\delta + \gamma}, \quad (12)$$

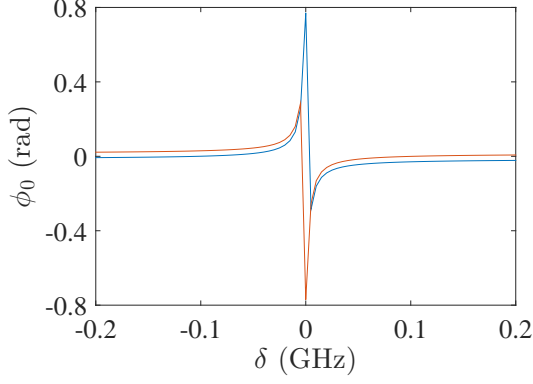


Figure 3: (Color online) Matching phase angle ϕ_0 versus the atom-cavity detuning δ for the two branches of steady states of $\langle x \rangle$. The color of the curve matches that of its corresponding curve of $\langle x \rangle$ in Fig. 2.

where a and b denote the cavity mode and the atom bosonic mode, respectively, in their dual space. \mathfrak{F} denotes the noise input associated with the dissipation term γb . Substituting Eq. (12) into the Laplace transform of Eq. (4) and ignoring the noise input associated with the cavity linewidth κ as it is irrelevant to the cavity's response to the motion of the atomic ensemble, we find the cavity mode as the inverse Laplace transform

$$a(t) = \mathcal{L}^{-1} \left\{ \frac{-iG e^{i\phi} \mathfrak{F}}{(s - i\eta x + \kappa)(s + i\delta + \gamma) + G^2 e^{2i\phi}} \right\}. \quad (13)$$

The denominator of Eq. (13) is a quadratic equation of s whose two roots will become the coefficients of time in exponentials through the inverse transform. Hence, the real parts of the roots will signify the amplification or attenuation of the cavity mode while the imaginary parts only contribute to the dispersed oscillations of the cavity mode. For the atom-cavity coupling to set off the loss in the cavity and the atomic modes and contribute a net gain to the dynamic system, one requires from this quadratic equation that the inequality

$$\begin{aligned} \sin^2 2\phi + \frac{\kappa - \gamma}{G} \frac{\delta + \eta x}{G} \sin 2\phi - \left(\frac{\kappa + \gamma}{G} \right)^2 \cos 2\phi \\ \geq \frac{\kappa \gamma}{G^2} \left[\left(\frac{\kappa + \gamma}{G} \right)^2 + \left(\frac{\delta + \eta x}{G} \right)^2 \right] \end{aligned} \quad (14)$$

regarding the phase factor $G e^{i\phi}$ is satisfied (see Appendix for the detailed derivation).

Shown in Fig. 4, the contour plots illustrate the inequality through the difference between the terms on the left and on the right hand sides of Eq. (14) against the variables δ , G and ϕ , such that the contour levels that are greater than zero (circled by the white dashed curves) indicate the region where Eq. (14) is satisfied, i.e. where the atom-cavity interaction obtains a net gain. The system parameters used retain those used in Sec. III.A above. In particular, the vertical axis for G in the subfigure (a) corresponds to the exponential scaling of experimentally accessible atomic density from 10^3 to 10^6 . For

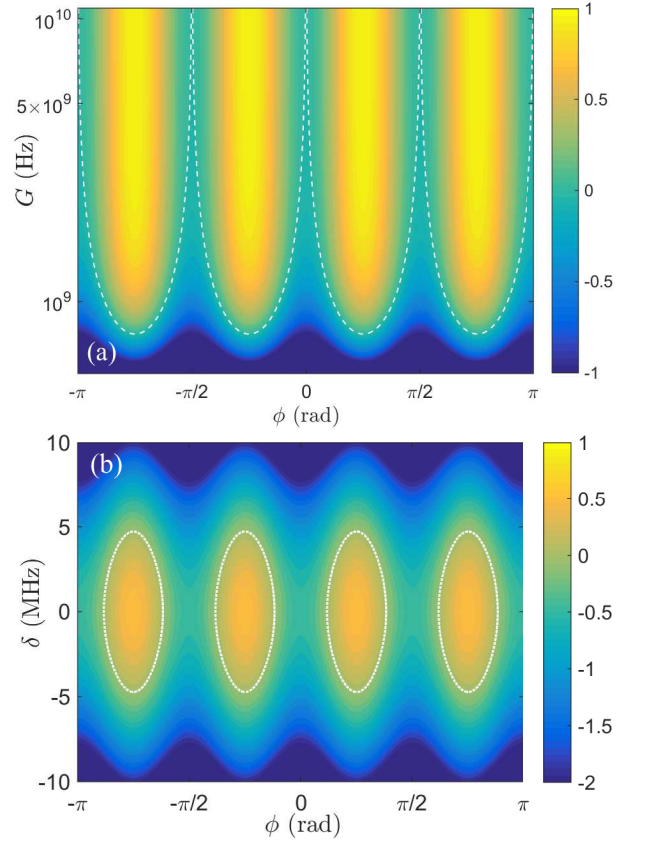


Figure 4: (Color online) Illustrating the atom-cavity gain regions through contour plots of the gain-loss inequality (a) as a function $F(G, \phi)$ against the atom-cavity coupling strength G and the phase ϕ at atom-cavity resonance $\delta = 0$; and (b) as a function $F(\delta, \phi)$ against the atom-cavity detuning δ and the phase ϕ at $G = 1\text{GHz}$. In (a), the vertical G axis is logarithmic to show the effect of exponential scaling of atomic density N . In both plots, the white dashed curves indicate the zero level, within which one obtains a net gain and without which one obtains a net loss to the optomechanical system.

the subfigure (b), we choose G to be 1GHz where the net gain regions just emerge.

The two plots here verify the analysis given in the last section that multistable regions emerge when the atom-cavity coupling is strong enough to overcome their individual dissipations to the environment. The loss-to-gain transitions in the contours (the white dashed curves) coincides with the phase-matching value of Eq. (8) for which the dynamic gain-loss balance between the atomic ensemble and the cavity field as given in Eq. (6) is obtained. The atoms therefore plays the active role under which the stable values admissible to the mirror's coordinate $\langle x \rangle$ can be dynamically traced along the paths of Fig. 2 through tuning the phase ϕ_0 and the detuning δ along a fixed contour in Fig. 4.

Moreover, shown in subfigure (a), the net gain regions expand when G is increased and the regions become asymptotically connected when G approaches to infinitely large. Correspondingly in subfigure (b), stronger coupling G leads to both longer major and longer minor axes in the elliptical

net-gain regions. The strong-coupling effect is more exemplified in the major axis, signifying a larger tolerance range of gain about the detuning. No matter the net-gain regions shrink or expand, their centers remain fixated at the atom-cavity resonance on one axis and at the points where $\phi = [\pm \tan^{-1}(G^2/\kappa\gamma) + k\pi]/2$ on the other, the latter of which is reduced from Eq. (8) when δ is set to 0. Coinciding with the peaks of ϕ in Fig. 3, these periodic points in ϕ are invariable with respect to G and form the dynamical attractors of the mirror's oscillation in the optomechanical cavity.

IV. HYSTERSIS CYCLES

When studying the multistability of a dielectric in an FP cavity, the high-order susceptibility of the dielectric translates into a multi-response of the classical medium to an input driving field. This multi-response is reflected graphically as a hysteresis cycle in the input-output plot where the incident field strength or its variants is regarded as the input and the transmitted field strength or its variants as the output. Depending on the absorptive response of the susceptibility, different shapes of hysteresis cycles will result, determining the existence of multistability and characterizing the multistability if it does exist. For example, in one respect, the absorptivity of the medium is reflected by the area enclosed in the hysteresis cycle. [2]

Here, we treat the coordinate quadrature $X_{\langle b \rangle} = \langle b \rangle + \langle b^\dagger \rangle$ of the steady state of the atomic ensemble as the driving input and the coordinate quadrature $X_{\langle a \rangle} = \langle a \rangle + \langle a^\dagger \rangle$ of the cavity field as output to examine the hysteresis cycle. From Eq. (4), the steady-state value $\langle a \rangle$ is proportional to $\langle b \rangle$. Converting the variable dependence and substituting the steady-state of the mirror $\langle x \rangle$ from Eq. (3), we have

$$\langle b \rangle = \frac{1}{Ge^{i\phi}} \left[\frac{\eta^2 |\langle a \rangle|^2}{m\omega_M^2} + i\kappa \right] \langle a \rangle. \quad (15)$$

Thus, besides a constant phase difference introduced by the proportional coefficient, the variation of $\langle b \rangle$ is in-phase with the variation of $\langle a \rangle$.

The equations of motion Eq. (3)- (5) do not determine this common phase shared by $\langle a \rangle$ and $\langle b \rangle$ since the steady states constrained by the gain-loss balance in Eq. (6) make the matrix equation in Eq. (11) self-consistent, thereby leaving an undetermined degree of freedom in this phase. To simplify our discussions below, we choose zero for this phase such that $\langle a \rangle = \langle a^\dagger \rangle = |\langle a \rangle|$. The quadrature of the atomic bosonic mode can hence be written as

$$X_{\langle b \rangle} = X_{\langle a \rangle} \left[\frac{\eta^2 X_{\langle a \rangle}^2}{4Gm\omega_M^2} \cos \phi + \frac{\kappa}{G} \sin \phi \right], \quad (16)$$

in a form reminiscent to the hysteresis cycle of static bistability for a dielectric in a FP cavity.

However, the three-order polynomial on the right hand side of the equation not only gives rise to a bi-valuation of $X_{\langle b \rangle}$ at a given $X_{\langle a \rangle}$ because the phase ϕ at the steady state of $\langle x \rangle$ can admit multiple values constrained only by the coupling

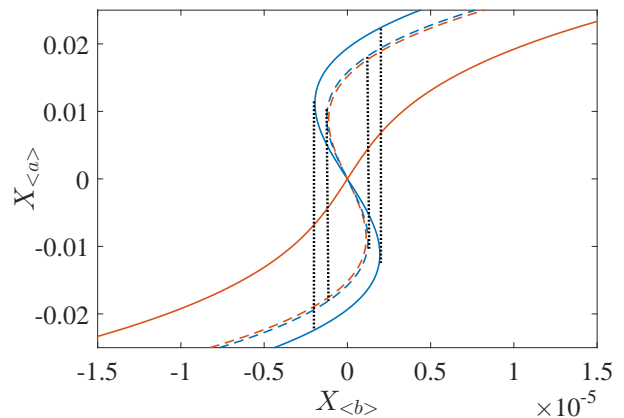


Figure 5: (Color online) Hysteresis cycles formed in the quadrature output $X_{\langle a \rangle}$ in the cavity field versus the quadrature input $X_{\langle b \rangle}$ in the atomic mode at atom-cavity resonance $\delta = 0$ (solid curves) and at small detuning $\delta = -1.5$ MHz (dashed curves). The black dotted lines serve as visual guides for the cycles formed. The blue curves (solid and dashed) correspond to the upper branch of $\langle x \rangle$ while the orange curves (solid and dashed) correspond to the lower branch of $\langle x \rangle$ in Fig. 2.

strength G as given in Eq. (8). Besides the periodicity allowed by the integer values of k , ϕ_0 can admit two values along the two branches of $\langle x \rangle$ for a fixed k , therefore giving rise to quadruple-valuation of $X_{\langle b \rangle}$ if G is given appropriate values. This is shown in Fig. 5 as two differently colored curves where $k = 0$ and G is chosen to be 345 MHz. The detuning δ is chosen at two typical values: $\delta = 0$ and $\delta = -1.5$ MHz.

At resonance, the upper branch of $\langle x \rangle$ associates with two bistable values of $X_{\langle b \rangle}$ while the lower branch of $\langle x \rangle$, though itself being mono-valued, adds a third valuation to $X_{\langle b \rangle}$, making the system tristable. Departing from resonance, the values of $X_{\langle b \rangle}$ associated with the two branches of $\langle x \rangle$ converge, exhibiting bistability for both branches, making the system quadruply stable, shown as the dashed curves in the figure. We note that the asymmetric dependence of ϕ on δ leads to an asymmetric dependence of the hysteresis cycles on δ , i.e. the hysteresis cycles vanish at $\delta = 1.5$ MHz.

V. CONCLUSIONS

Using a hypothetical Hamiltonian whose interaction part has broken \mathcal{PT} -symmetry, we show that periodical multistable states can exhibit in an atom-filled optomechanical cavity when the periodicity matches a gain or loss balance between the filled atomic ensemble and the cavity field. Unlike the multistability arises in FP cavity, the atoms whose motion is described by a bosonic mode plays an active role in developing the multistable states. When the gain brought by the atoms into the cavity exactly counter-act against the loss of all components in the cavity, the mechanical mirror is driven from zero state into two branches that match with the amount of gain dynamically obtained.

Since traditional studies on multistability strongly focus on

the controllability of optical systems, the dynamically tuned multistability developed here can be viewed as an extra level of control one can exert on optical cavity systems without the interference of an external driving laser.

We also note that the collapse of the hysteresis cycles, i.e. transition from multi-valuation to mono-valuation of input-output, shown in Fig. 5 is not continuous with respect to the detuning δ and we leave the investigation of this discontinuity in transition to future studies.

Appendix A: Weighing gain through Laplace transforms

The denominator in the inverse Laplace transform of Eq. (13) is the quadratic polynomial

$$s^2 + [\kappa + \gamma + i(\delta - \eta\mathfrak{x})]s + \delta\eta\mathfrak{x} + \kappa\gamma + i(\delta\kappa - \gamma\eta\mathfrak{x}) + G^2 e^{2i\phi} \quad (\text{A1})$$

whose zeros will concern the determination of gain and loss of the cavity field contributed by the atom-cavity interaction. Since the coefficient of the linear term of the polynomial is independent of G and ϕ , we need only consider the discriminant of the roots. Writing the phase $e^{2i\phi}$ in rectangular coordinate form and combining it with the other terms, we find the complex discriminant to be

$$\mathcal{D} = (\kappa - \gamma)^2 - (\delta + \eta\mathfrak{x})^2 - 4G^2 \cos 2\phi - 2i [(\kappa - \gamma)(\delta + \eta\mathfrak{x}) + 2G^2 \sin 2\phi].$$

Introducing the abbreviations $\kappa_\gamma = \kappa - \gamma$ and $\delta_\eta = \delta + \eta\langle x \rangle$, it reads in polar form

$$\mathcal{D} = 4G^2 \exp\{-i\theta\} \times \sqrt{1 - \left[\frac{\kappa_\gamma^2 - \delta_\eta^2}{2G^2} \cos 2\phi - \frac{\kappa_\gamma \delta_\eta}{G^2} \sin 2\phi \right] + \left(\frac{\kappa_\gamma^2 + \delta_\eta^2}{4G^2} \right)^2}$$

where

$$\theta = \tan^{-1} \frac{2\kappa_\gamma \delta_\eta + 4G^2 \sin 2\phi}{\kappa_\gamma^2 - \delta_\eta^2 - 4G^2 \cos 2\phi} + k\pi \quad (\text{A2})$$

for all $k \in \mathbb{Z}$.

The sign of the real part of $\sqrt{\mathcal{D}}$, concerning the amplification and attenuation, is determined by the sign of $\cos(\theta/2)$. Considering that we let the arctangent take value between $-\pi/2$ and $\pi/2$ only, $\cos(\theta/2)$ would be positive and if k is either 0 or even and negative if k is odd. Therefore, as a part of a root, the sign of $\sqrt{\mathcal{D}}$ is independent of the values G and ϕ take but is dependent on the sign of the square root takes, with the positive corresponds to the upper branch and the negative corresponds to the lower branch of Fig. 2.

To decide whether the positive branch can contribute a net gain to the atom-driven mirror oscillation, we compare its value to the decay contributed by the cavity and the atoms themselves (the real part of the linear term in Eq. (A1)), i.e.

$$\Re\{\sqrt{\mathcal{D}}\} \geq \kappa + \gamma.$$

Shuffling the terms, we arrive at the inequality

$$(G^2 \sin 2\phi)^2 + (\kappa - \gamma)\delta_\eta G^2 \sin 2\phi - (\kappa + \gamma)^2 G^2 \cos 2\phi \geq \kappa\gamma [(\kappa + \gamma)^2 + \delta_\eta^2].$$

Dividing all the terms by G^4 gives Eq. (14). At the steady state, one has from the balance equation given in Eq. (6) that

$$\begin{aligned} G^2 \cos 2\phi &= -\kappa\gamma - \delta_\eta \langle x \rangle, \\ G^2 \sin 2\phi &= -\kappa\delta + \gamma\eta \langle x \rangle, \end{aligned}$$

for which one can verify that the equality sign is obtained, i.e. $\Re\{\sqrt{\mathcal{D}}\} = \kappa + \gamma$.

Acknowledgments

The research presented is supported by FDCT of Macau under grant 013/2013/A1, University of Macau under grants MRG022/IH/2013/FST and MYRG2014-00052-FST, and National Natural Science Foundation of China under grant No. 11404415.

-
- [1] H. M. Gibbs, S. L. McCall, and T. N. C. Venkatesan, Phys. Rev. Lett. **36**, 1135 (1976); H. M. Gibbs, F. A. Hopf, D. L. Kaplan, and R. L. Shoemaker, *ibid.* **46**, 474 (1981).
 - [2] H. Gibbs, *Optical Bistability: Controlling Light With Light* (Elsevier, 1985).
 - [3] R. Bonifacio and L. A. Lugiato, Phys. Rev. A **18**, 1129 (1978); R. Bonifacio and P. Meystre, Optics Communications **29**, 131 (1979).
 - [4] J. H. Marburger and F. S. Felber, Phys. Rev. A **17**, 335 (1978).
 - [5] M. Kitano, T. Yabuzaki, and T. Ogawa, Phys. Rev. Lett. **46**, 926 (1981).
 - [6] A. Joshi and M. Xiao, Phys. Rev. Lett. **91**, 143904 (2003).
 - [7] P. Meystre, E. M. Wright, J. D. McCullen, and E. Vignes, J. Opt. Soc. Am. B **2**, 1830 (1985).
 - [8] Z. R. Gong, H. Ian, Y. Liu, C. P. Sun, and F. Nori, Phys. Rev. A **80**, 065801 (2009).
 - [9] A. B. Klimov, L. L. Sánchez-Soto, and J. Delgado, Optics Communications **191**, 419 (2001).
 - [10] A. Dorsel, J. D. McCullen, P. Meystre, E. Vignes, and H. Walther, Phys. Rev. Lett. **51**, 1550 (1983).
 - [11] F. Marquardt, J. G. E. Harris, and S. M. Girvin, Phys. Rev. Lett. **96**, 103901 (2006).
 - [12] Y. Chang, T. Shi, Y. Liu, C. P. Sun, and F. Nori, Phys. Rev. A **83**, 063826 (2011).
 - [13] F. Marquardt and S. M. Girvin, Physics **2**, 40 (2009).
 - [14] J. Qian, A. A. Clerk, K. Hammerer, and F. Marquardt, Phys.

- Rev. Lett. **109**, 253601 (2012).
- [15] R. Ghobadi, A. R. Bahrapour, and C. Simon, Phys. Rev. A **84**, 033846 (2011).
- [16] T. Huan, R. Zhou, and H. Ian, Phys. Rev. A **92**, 022301 (2015).
- [17] Y. Dong, J. Ye, and H. Pu, Phys. Rev. A **83**, 031608 (2011).
- [18] G. S. Agarwal and S. Huang, Phys. Rev. A **81**, 041803 (2010).
- [19] A. Kronwald and F. Marquardt, Phys. Rev. Lett. **111**, 133601 (2013).
- [20] M. Karuza, C. Biancofiore, M. Bawaj, C. Molinelli, M. Galassi, R. Natali, P. Tombesi, G. Di Giuseppe, and D. Vitali, Phys. Rev. A **88**, 013804 (2013).
- [21] M. Wallquist, K. Hammerer, P. Zoller, C. Genes, M. Ludwig, F. Marquardt, P. Treutlein, J. Ye, and H. J. Kimble, Phys. Rev. A **81**, 023816 (2010).
- [22] D. Hunger, S. Camerer, T. W. Hänsch, D. König, J. P. Kotthaus, J. Reichel, and P. Treutlein, Phys. Rev. Lett. **104**, 143002 (2010).
- [23] K. Zhang, W. Chen, M. Bhattacharya, and P. Meystre, Phys. Rev. A **81**, 013802 (2010).
- [24] F. Brennecke, S. Ritter, T. Donner, and T. Esslinger, Science **322**, 235 (2008).
- [25] H. Ian, Z. R. Gong, Y. Liu, C. P. Sun, and F. Nori, Phys. Rev. A **78**, 013824 (2008).
- [26] F. Brennecke, T. Donner, S. Ritter, T. Bourdel, M. Köhl, and T. Esslinger, Nature **450**, 268 (2007).
- [27] J. J. Hopfield, Phys. Rev. **112**, 1555 (1958).
- [28] C. M. Bender and S. Boettcher, Phys. Rev. Lett. **80**, 5243 (1998).
- [29] H. Jing, S. K. Özdemir, X.-Y. Lü, J. Zhang, L. Yang, and F. Nori, Phys. Rev. Lett. **113**, 053604 (2014).
- [30] C. M. Bender, M. Gianfreda, Ş. K. Özdemir, B. Peng, and L. Yang, Phys. Rev. A **88**, 062111 (2013).
- [31] B. Peng, Ş. K. Özdemir, F. Lei, F. Monifi, M. Gianfreda, G. L. Long, S. Fan, F. Nori, C. M. Bender, and L. Yang, Nat. Phys. **10**, 394 (2014).
- [32] X.-Y. Lü, H. Jing, J.-Y. Ma, and Y. Wu, Phys. Rev. Lett. **114**, 253601 (2015).
- [33] Y. Colombe, T. Steinmetz, G. Dubois, F. Linke, D. Hunger, and J. Reichel, Nature **450**, 272 (2007).
- [34] P. R. Hemmer, N. P. Bigelow, D. P. Katz, M. S. Shahriar, L. DeSalvo, and R. Bonifacio, Phys. Rev. Lett. **77**, 1468 (1996).
- [35] R. Bonifacio, L. De Salvo, L. M. Narducci, and E. J. D'Angelo, Phys. Rev. A **50**, 1716 (1994).
- [36] J. Javaloyes, M. Perrin, and A. Politi, Phys. Rev. E **78**, 011108 (2008).